Applied Catalysis B: Environmental 156–157 (2014) 72–83

Contents lists available at ScienceDirect

Applied Catalysis B: Environmental

journal homepage: www.elsevier.com/locate/apcatb

Selective catalytic reduction of NO_x by hydrogen (H_2-SCR) on WO_x-promoted $Ce_zZr_{1-z}O_2$ solids

Ari Väliheikki[a], Klito C. Petallidou[b], Christos M. Kalamaras[b], Tanja Kolli[a], Mika Huuhtanen[a], Teuvo Maunula[c], Riitta L. Keiski[a], Angelos M. Efstathiou[b,*]

[a] Mass and Heat Transfer Process Laboratory, Department of Process and Environmental Engineering, P.O. Box 4300, FI-90014 University of Oulu, Finland
[b] Department of Chemistry, University of Cyprus P.O. Box 20537, University Campus, 1678 Nicosia, Cyprus
[c] Dinex Ecocat Oy, Product Development, Typpitie 1, FI-90620 Oulu, Finland

ARTICLE INFO

Article history:
Received 17 October 2013
Received in revised form 9 February 2014
Accepted 4 March 2014
Available online 13 March 2014

Keywords:
Selective catalytic reduction
H_2-SCR
Surface acidity
NH_3-TPD
Tungsten
NO-TPD
H_2/O_2-TPSR
UV–vis/DRS
Nitrogen oxides

ABSTRACT

The selective catalytic reduction of NO_x by H_2 (H_2-SCR) under strongly oxidizing conditions (520 ppm NO_x/1% H_2/5% O_2/10% CO_2/He; NO:NO_2–4:1–9:1) in the 150–600 °C range has been studied over 3 wt-% W-promoted CeO_2–ZrO_2 solids (85 wt-% CeO_2-15 wt-% ZrO_2 (CeZr), and 17 wt-% CeO_2–83 wt-% Zr (ZrCe) synthesised by a proprietary method) for the first time. The highest NO_x conversion (X_{NO_x} = 54%) was obtained on the W-ZrCe (Zr-rich) solid at 300 °C (GHSV of 51,000 h^{-1}), whereas N_2-selectivity was in the 77–92%-range over both W-ZrCe (Zr-rich) and W-CeZr (Ce-rich) catalysts. Significantly higher integral specific rates (R_{NO}, μmol NO m^{-2} min^{-1}) were estimated on the W-ZrCe (Zr-rich) catalyst compared to the W-CeZr (Ce-rich) one in the 250–350 °C range. The formation of adsorbed NO_x under 0.1% NO/10% O_2/He gas treatment at 25 °C followed by H_2/O_2-TPSR experiments revealed that at least two different kinds of active NO_x of low concentration (4–7 μmol g^{-1}) were formed on both catalysts, whereas other inactive (spectator) NO_x species formed were of larger concentration (>160 μmol g^{-1}). UV–vis/DRS studies revealed that deposition of 3 wt-% W on ZrCe (Zr-rich) mixed metal oxide following calcination at 600 °C resulted in the formation of both polymeric WO_x and WO_3 clusters, whereas on CeZr (Ce-rich) only the latter phase (W^{6+}) was seen. Large differences in the concentration (μmol m^{-2}) and strength of surface acid sites between the W-CeZr and W-ZrCe solids were revealed after performing NH_3-TPD and NH_3-DRIFTS. These results were found to correlate with the specific H_2-SCR rate (μmol m^{-2} min) obtained for the two solids. In particular, the surface acid sites on W-ZrCe and W-CeZr solids were found to be 5.96 and 2.76 μmol m^{-2}, respectively, whereas the specific reaction rate was 0.14 and 0.046 μmol m^{-2} min at 300 and 250 °C, at which maximum rates were observed, respectively.

1. Introduction

Nitrogen oxide (NO_x) emissions from mobile and stationary sources are major concern due to their effect on human health and the environment. This has led to stringent legislation for reducing NO_x emissions during the last decades [1]. Selective catalytic reduction (SCR) has proven to be an effective method for reducing NO_x emissions, where different reducing agents such as ammonia (NH_3) and urea ($OC(NH_2)_2$) [2–6] as well as hydrocarbons (HCs) [7–10] and hydrogen (H_2) [11–16] have been applied. The most commonly used reducing agent is ammonia, and the NH_3-SCR technology has been applied since 1973 [17–21]. However, the today's great concerns about the increasing emissions of carbon dioxide to the atmosphere, and problems faced by the current NH_3-SCR technology, such as ammonia slip, ash odor, air-heaters fouling and high running cost, demand the finding of appropriate non carbon-containing reducing agents for the catalytic removal of NO_x from combustion exhaust streams, and preferably at low temperatures for reduced operational and investment costs [22,23]. Until the full transition to the hydrogen economy and zero emissions of greenhouse gases are achieved, H_2-SCR might be considered as a breakthrough NO_x control technology in favour of the present NH_3-SCR, especially applied at industrial sites where H_2 gas is available (e.g. olefin plants, petrochemical plants, oil refineries, hydrogen plants, etc.) [16]. Hydrogen-assisted NH_3-SCR and urea-SCR are

* Corresponding author. Tel.: +357 22892776; fax: +357 22892801.
E-mail addresses: riitta.keiski@oulu.fi (R.L. Keiski), efstath@ucy.ac.cy (A.M. Efstathiou).

http://dx.doi.org/10.1016/j.apcatb.2014.03.008
0926-3373/

gaining an increasing interest in recent years [24–27] due to an impressive enhancement in NO_x conversion over the $Ag/\gamma\text{-}Al_2O_3$ catalyst for mobile NO_x control applications.

Supported noble metal (Pt and Pd) catalysts have proven to be efficient for reducing NO_x emissions in H_2-SCR [11–13,28–31]. Yu et al. [31] have reported high NO_x conversions (over 90%) on a Pd/SiO_2 catalyst at 170–300 °C. Similar results have also been reported [11] on $Pt/MgO\text{-}CeO_2$ with 95% NO conversion at 150 °C and N_2 selectivities of 78–92% in the 100–400 °C range. In addition, the mechanism of H_2-SCR of NO on supported Pt catalysts has been extensively studied by SSITKA-Mass spectrometry, SSITKA-DRIFTS and various transient isotopic coupled with TPSR techniques [11,12,32–35]. Due to the high price and limited availability of noble metals, alternative suitable catalytic materials such as metal oxides pose as a big challenge for investigation towards H_2-SCR. To our knowledge, no reports appear in the open literature regarding H_2-SCR of NO_x on metal oxide surfaces.

Ceria-zirconia-based mixed metal oxides or solid solutions have found important applications in exhaust gas after treatment, such as in three-way catalysts (TWCs), SCR and diesel oxidation catalysts (DOC) due mainly to their high oxygen storage capacity (OSC) [36]. In addition, ceria (CeO_2) has good redox properties [36–40] but the incorporation of Zr^{4+} into its crystal lattice (formation of solid solution) results in a significant increase in the reducibility of ceria ($Ce^{4+} \leftrightarrow Ce^{3+}$) [36,40–44], improves its thermal stability, and prevents sintering of the resulting $Ce_{1-x}Zr_xO_{2-\delta}$ solid [45], which are important factors for the SCR of NO_x. In particular, Cu-Ce-Zr-O mixed metal oxides have shown almost complete NO conversion at 300–500 °C in NH_3-SCR [41]. When tungsten (W) was added in cerium oxide-based catalysts, promising materials towards NH_3-SCR were found [3,4,6]. Tungsten oxide-promoted ZrO_2 catalysts have been studied for CH_4-SCR of NO_x [46]. However, for other SCR applications the tungsten-cerium-zirconium mixed oxide catalysts have not been yet studied widely. Li et al. [47] and Väliheikki et al. [48] have recently reported on the good performance of tungsten-loaded cerium-zirconium oxide catalysts in NH_3-SCR.

The aim of this study is to gain new knowledge about the suitability of cerium-zirconium-based mixed metal oxides towards H_2-SCR of NO_x. On the basis of this knowledge, one of the further goals is to develop catalysts suitable for H_2-assisted NH_3-SCR for mobile and stationary applications. Two different tungsten (W) loaded cerium-zirconium mixed metal oxides (Ce-rich and Zr-rich) were prepared. The catalysts were characterized for (a) surface texture (BET/BJH method), (b) surface acidity and NO_x adsorption by temperature programmed desorption (TPD) of NH_3 and NO, respectively, (c) NO_x reactivity towards hydrogen in the presence of oxygen by temperature-programmed surface reaction (H_2/O_2-TPSR), (d) W oxidation states and energy band gaps by ultraviolet–visible spectroscopy (UV–vis/DRS), and (e) acid sites quality by NH_3-DRIFTS followed by TPD. These studies enabled to draw reasonable conclusions regarding the link between H_2-SCR of NO_x performance and some surface physico-chemical properties of the CeO_2-ZrO_2-based mixed metal oxides.

2. Experimental

2.1. Catalyst preparation

The Zr-rich cerium-zirconium oxide (ZrCe) and Ce-rich cerium-zirconium oxide (CeZr) supports were provided by Dinex Ecocat Oy (Finland). The chemical composition was 85 wt-% CeO_2–15 wt-% ZrO_2 (CeZr), and 17 wt-% CeO_2–83 wt-% ZrO_2 (ZrCe) synthesised by a proprietary method. The 3 wt-% W-supported catalysts (W-ZrCe and W-CeZr) were prepared by the wet impregnation method using ammonium metatungstate hydrate ($(NH_4)_6H_2W_{12}O_{40}\cdot xH_2O$, 99.99%, Sigma Aldrich) as the precursor compound. An appropriate amount of precursor (0.483 g) was dissolved in distilled water (10 mL) and then added with the support (11.640 g) in 110 mL of distilled water. The resulting solution in the case of W-CeZr (initial pH 2.1) or W-ZrCe (initial pH 7.6) was continuously agitated with a magnetic stirrer overnight at 50 °C. The sample was then dried overnight at 120 °C. Finally, the catalyst was calcined in static air in a muffle oven for 1 h at 150 °C, 2 h at 350 °C and 1 h at 600 °C using a heating rate of 5 °C min^{-1} between the steps.

Table 1
BET surface area, single point BJH pore volume, and BJH pore size over W-ZrCe and W-CeZr catalysts as well as ZrCe and CeZr supports.

Catalyst/Support	BET surface area, S_{BET} ($m^2\ g^{-1}$)	Single point BJH pore volume ($cm^3\ g^{-1}$)	BJH mean pore size (nm)
W-ZrCe	67.2	0.173	10.3
W-CeZr	91.9	0.168	7.3
ZrCe	56.0	0.133	9.5
CeZr	98.1	0.155	6.3

2.2. Catalyst characterization

2.2.1. Surface texture

The specific surface area ($m^2\ g^{-1}$), mean pore size (nm) and pore volume ($cm^3\ g^{-1}$) of the CeZr and ZrCe supports as well as W-ZrCe and W-CeZr catalysts were determined by N_2 adsorption at 77 K (Micrometrics ASAP2020 analyser). The Brunauer–Emmett–Teller (BET) method was used for determining the specific surface areas (S_{BET}, $m^2\ g^{-1}$) and the Barrett–Jolenda–Halenda (BJH) method for determining the pore volumes and mean pore diameters of the solids. BET specific surface areas, pore volumes and mean pore sizes for the W-ZrCe and W-CeZr catalysts are presented in Table 1. The Ce/Zr atom ratio in the catalyst support composition affected both the BET surface area and the mean pore size. The W-CeZr catalyst exhibits 37 and 41% higher BET surface area and mean pore size, respectively than the W-ZrCe catalyst. Differences observed between the pore volumes of the two catalysts were, however, small. The addition of WO_x on ZrCe mixed metal oxide increased the BET surface area and pore size by 20 and 8%, respectively. On the other hand, WO_x addition on CeZr mixed metal oxide decreased slightly (by 6%) the BET surface area but increased the pore volume by 16%.

2.2.2. Powder X-ray diffraction studies

Powder X-ray diffraction patterns were recorded in the 20–80° 2θ range (scan speed = 1° min^{-1}) using a Rigaku Miniflex powder X-ray diffractometer with Ni-filtered Cu Kα radiation (λ = 1.5418 Å) operating at 30 kV and 15 mA. The XRD pattern of the W-CeZr solid showed diffraction peaks at 2θ = 28.8, 33.5, 48.0, 57.0, 59.8, 70.2, and 77.7, slightly shifted from those corresponding to the pure CeO_2 crystal structure (2θ = 28.7, 33.1, 47.5, 56.2, 59.2, 69.7, 76.7°). For the W-ZrCe solid, the diffraction peaks obtained at 2θ = 30.0, 34.9, 50.1, 59.7, 62.5, and 72.6 were further shifted to higher 2θ angles with respect to W-CeZr due to the introduction of more Zr^{4+} into the ceria lattice. In addition to the Ce-Zr-O solid solution formed, the diffraction peaks of the tetragonal zirconia (t-ZrO_2) phase were seen [49]. The absence of WO_3 diffraction peaks is due to the low quantity and/or the very small mean primary crystal size of this phase which cannot be detected by powder XRD. Based on the Scherrer equation [50], the primary crystal size (nm) of the CeZr and ZrCe solid solutions was estimated. The latter was found to be 5.4 and 6.7 nm for the CeZr and W-CeZr, respectively. Similar particle sizes (10.3 nm) were found for the ZrCe and W-ZrCe solids.

Table 2
Sequential step changes in feed gas composition during NH_3-TPD, NO-TPD and H_2/O_2-TPSR experiments.

Experiment	Sequence of step changes in gas flow
NH_3-TPD	1.11% NH_3/He (30 min, 25 °C) → He (15 min, 25 °C) → TPD in He flow (30 °C min^{-1})
NO-TPD	0.1% NO/He (30 min, 25 °C) → He (15 min, 25 °C) → TPD in He flow (30 °C min^{-1})
H_2/O_2-TPSR	0.1% NO/10% O_2/He (30 min, 25 °C) → He (15 min, 25 °C) → TPSR in 1% H_2/5% O_2/He flow (30 °C min^{-1})

2.2.3. TPD and TPSR

Temperature-programmed desorption (TPD) following NO (0.1% NO/He, 25 °C, 100 mL min^{-1}) or NH_3 (1.1% NH_3/He, 25 °C, 30 mL min^{-1}) chemisorption, and temperature- programmed surface reaction (TPSR) in 1% H_2/5% O_2/He (30 mL min^{-1}) gas flow following 0.1% NO/10% O_2/He gas treatment (100 mL min^{-1}) of the catalyst at 25 °C were conducted in a specially designed gas flow-system and a quartz microreactor described elsewhere [51]. The amount of catalyst used was 0.3 g and the total flow rate of the inert gas (He) was 30 NmL min^{-1} during the TPD experiments. Chemical analysis of the gas effluent flow from the reactor was performed with an *on line* quadrupole mass spectrometer (Omnistar, 1-300 amu, Balzers) equipped with a fast response inlet capillary/leak valve (SVI 050, Balzers) and data acquisition systems. The mass numbers (m/z) 2, 15, 28, 30, 44 and 46 were used for continuously monitoring H_2, NH_3, N_2, NO, N_2O and NO_2, respectively. The MS signals were calibrated against standard gas mixtures. For the estimation of the NO concentration, the contribution of NO_2 to $m/z = 30$ was considered.

Before a given temperature-programmed experiment, the W-ZrCe or W-CeZr catalyst was calcined in situ (20% O_2/He) at 600 °C for 1 h followed by He purge for 10 min at 600 °C and cooling of the reactor in a He flow to 25 °C. Table 2 describes the necessary sequence of step changes in gas composition in each temperature-programmed experiment performed. It is noted that the different NO chemisorption conditions applied before NO-TPD and TPSR allow to probing the effect of oxygen on the kinds of adsorbed NO_x formed but also the reactivity of them under similar H_2-SCR conditions.

2.2.4. NH_3-DRIFTS studies

In situ DRIFT spectra following NH_3 chemisorption at 25 °C and temperature-programmed desorption (NH_3-TPD) under Ar flow were recorded using a Perkin-Elmer Frontier FT-IR spectrometer (126 scans per averaged spectrum, resolution of 4 cm^{-1}, scan speed of 5 scans s^{-1}) equipped with a high-temperature/high-pressure temperature controllable DRIFTS cell (Harrick, Praying Mantis). The W-CeZr or W-ZrCe solid sample (~80 mg) in a very fine powder form was placed firmly into the ceramic cup of the DRIFTS cell, calcined at 600 °C for 1 h (20 vol% O_2/He), and then purged in Ar flow. The spectrum of the solid in Ar gas flow was then recorded at the desired temperature (25–600 °C), and subtracted from the spectrum of the solid recorded in 0.55%NH_3/Ar/He gas treatment at 25 °C or in Ar flow at higher temperatures during TPD. DRIFT spectra when necessary were smoothed to remove high frequency noise and further analyzed using the software Spectrum10 for Windows.

2.2.5. UV–vis/DRS studies

In situ UV–vis/DR spectra of the W-ZrCe, W-CeZr, ZrCe and CeZr solids were recorded with a Perkin-Elmer Lambda 950 spectrometer equipped with a high-temperature/high-pressure temperature controllable DRS cell (Harrick, Praying Mantis) in the 270–800 nm range. The catalyst sample was first pretreated in Ar gas flow (60 mL min^{-1}) at 150 °C for 1 h followed by cooling in Ar flow to 25 °C before spectra acquisition was performed. The spectrum of a high reflectance reference material (fluorilon) was recorded at 25 °C and it was then subtracted from the spectrum of the solid. The Kubelka–Munk function, $F(R_\infty)$ was used to convert the sample's reflectance (R_{sample}) to pseudo-absorbance units using the following Eqs. (1) and (2) [52–54]:

$$R_\infty = \frac{R_{sample}}{R_{reference}} \quad (1)$$

$$F(R_\infty) = \frac{(1 - R_\infty)^2}{2R_\infty} \quad (2)$$

where R_{sample} and $R_{reference}$ are the sample's reflectance and that of the reference material, respectively.

2.3. Catalytic performance studies

The flow system used for performing catalytic measurements for the H_2-SCR of NO_x at 1 atm total pressure was previously described [51]. The effluent gas stream from the reactor was analysed *on line* using: (i) a NO_x chemiluminescence analyser (Thermo Electron Corporation, model 42 C) for NO and NO_2, (ii) a mass spectrometer (Balzers Omnistar) for H_2 ($m/z = 2$), and (iii) a N_2O infrared analyser (Teledyne Analytical Instruments, Model IR 7000). The amount of W-ZrCe and W-CeZr catalysts used was 0.33 and 0.66 g, respectively, and the total flow rate was 300 NmL min^{-1}, resulting in a GHSV of ~51,000 h^{-1} ($L/L_{cat}/h$), the same for each catalyst sample; the different densities for the two catalytic beds is noted. The prepared W-ZrCe and W-CeZr catalyst samples were first pretreated in situ under 20% O_2/He gas flow (50 mL min^{-1}) at 600 °C for 1 h. The reactor was then cooled in a He flow to 150 °C before activity measurements in the 150–600 °C range were initiated. The reaction feed gas stream consisted of 520 ppm NO_x (within 3% accuracy; NO:NO_2 ratio ~9:1), 1 vol% H_2, 5 vol% O_2, 10 vol% CO_2 and He as balance gas. Experiments were also performed in the presence of ~7 vol% H_2O (6.7–7.3 vol%) in the feed in the 250–350 °C range and at a GHSV of 51,000 h^{-1}.

The effect of GHSV (h^{-1}) on the performance of W-CeZr and W-ZrCe catalysts towards the H_2-SCR was also studied at 10,000 h^{-1} (vs. 51,000 h^{-1}) after adjusting the volume flow rate of the feed gas stream. The catalyst pre-treatment method and the reaction gas mixture composition were kept the same as mentioned above. In the case of GHSV of 10,000 h^{-1}, mass spectrometry was used to estimate NO conversion (based on $m/z = 30$) due to the low response time of the NO_x chemiluminescence analyser at the low gas-flow rate used. The effect of H_2 and O_2 feed concentrations were also investigated for the W-CeZr catalyst by testing three different H_2–O_2 feed gas compositions: (i) 1% H_2–5% O_2, (ii) 0.6% H_2–5% O_2 and (iii) 1% H_2–10% O_2 (NO:NO_2 = 4:1). Measurements were recorded after steady-state was achieved.

Blank activity measurements without the catalyst in place inside the reactor (gas-phase reaction) were performed and the concentrations of NO, N_2O and NO_2 recorded (e.g. due to oxidation of NO to NO_2) were subtracted from the results obtained with the catalyst in place inside the reactor. The NO_x conversion (X_{NO_x}) and H_2 conversion (X_{H_2}) were estimated via the following Eq. (3) and (4), respectively:

$$X_{NO_x} = \frac{\left(c_{NO,\,in} + c_{NO_2,\,in}\right) - \left(c_{NO,\,out} + c_{NO_2,\,out}\right)}{c_{NO,\,in} + c_{NO_2,\,in}} \times 100\% \quad (3)$$

$$X_{H_2} = \frac{c_{H_2,\,in} - c_{H_2,\,out}}{c_{H_2,\,in}} \times 100\% \quad (4)$$

where $c_{NO,in}$, $c_{NO_2,in}$, $c_{NO,out}$ and $c_{N_2O,out}$ depict the NO and NO_2 inlet and outlet concentrations of the reactor, respectively. Furthermore, $c_{H_2,in}$ and $c_{H_2,out}$ are the reactor's H_2 inlet and outlet

concentrations, respectively. The N_2 selectivity (S_{N_2}) of the H_2-SCR was estimated using Eq. (5):

$$S_{N_2} = \frac{(c_{NO_x,\,in} - c_{NO_x,\,out}) - 2 \times c_{N_2O,\,out}}{c_{NO_x,\,in} - c_{NO_x,\,out}} \times 100\% \quad (5)$$

where $c_{NO_x,in}$ and $c_{NO_x,out}$ are the NO_x concentrations in the inlet and outlet of the reactor, respectively. Furthermore, $c_{N_2O,out}$ depicts the N_2O concentration in the outlet of the reactor. No ammonia (NH_3) formation was noticed according to the measurement method applied [13]. The specific integral reaction rate of NO, R_{NO} (mol m^{-2} min^{-1}) was also estimated based on the NO conversion and considering the BET surface area (S_{BET}, m^2 g^{-1}) of the solid according to the following Eq. (6):

$$R_{NO} = \frac{\dot{F}^f_{NO} \times X_{NO}}{W_{cat} \times S_{BET}} \times 100\% \quad (6)$$

where $\dot{F}^f_{NO}$ is the molar flow rate of NO in the feed (mol NO min^{-1}), X_{NO} the conversion of NO (%), and W_{cat} is the mass of catalyst (g).

2.4. Absence of interphase and intraphase concentration gradients

The absence of interphase (external) concentration gradients was verified by the following diagnostic test [55]. For the GHSV of 51,000 h^{-1} used in all catalytic performance experiments, the linear velocity through the catalytic bed was varied (150 vs. 300 mL/min), and at the same time the catalyst volume (0.165 vs. 0.330 g) so as to keep the same GHSV (51,000 h^{-1}). For the gas composition used (see Section 2.3) and at the temperatures of 250 and 300 °C, where the maximum X_{NO} (%) was observed for the W-CeZr and W-ZrCe solids, respectively, the X_{NO} (%) estimated was very similar (within 3%) for the two conditions, thus verifying the absence of external mass transport resistances (constant X_{NO} with increasing linear velocity). The absence of *intraphase* (intraparticle) concentration gradients was verified by using two catalyst particle sizes. The first one was in the range $0.1 < d_p < 0.3$ mm (used in all catalytic performance studies), whereas the second particle size (d_p) was made smaller than 0.1 mm. At the temperatures of 250 and 300 °C, where the maximum X_{NO} (%) was observed for the W-CeZr and W-ZrCe solids, respectively, the NO conversion was very similar (within 5%) for both catalyst particles (use of 300 mL/min flow rate). This result proves the absence of *internal diffusion* resistances under the applied experimental conditions.

3. Results

3.1. Catalytic performance studies

3.1.1. NO_x conversion and N_2-selectivity vs. reaction temperature

Fig. 1 presents the conversions of NO_x (X_{NO_x}) and H_2 (X_{H_2}) over W-ZrCe and W-CeZr catalysts in the 150–600 °C range for a GHSV of 51,000 h^{-1}. Three temperature regions for NO_x reduction can be identified, namely: $T \leq 250$ °C, 300–350 °C, and $T \geq 400$ °C. The NO_x conversions obtained over the W-CeZr catalyst were between 8 and 20%-units higher below 250 °C, and less than 10%-units higher above 400 °C compared to the W-ZrCe catalyst. On the other hand, the opposite activity order was observed in the 300–350 °C range. In particular, W-ZrCe exhibits about 10%-units higher NO_x conversions than the W-CeZr catalyst. Maximum NO_x conversions of 54% and 46% were obtained for the W-ZrCe and W-CeZr catalysts at 300 and 250 °C, respectively (Fig. 1). It is very important to note here that the amount of W-ZrCe used was half that of W-CeZr in order to achieve the same GHSV (h^{-1}). The consequence of this on the catalyst's activity is illustrated below by considering the specific integral reaction rate (μmol NO m^{-2} min^{-1}) vs. temperature profile.

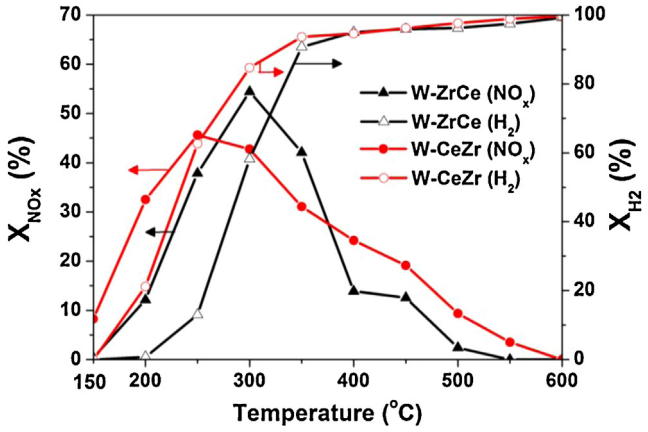

Fig. 1. NO_x conversion (X_{NO_x}, %) and H_2 conversion (X_{H_2}, %) in the H_2-SCR as a function of temperature over W-ZrCe and W-CeZr catalysts. Reaction conditions: 520 ppm NO_x (NO:NO_2 ~9:1), 1.0 vol% H_2, 5 vol% O_2, 10 vol% CO_2 and He as balance gas; GHSV ~51,000 h^{-1}; $m_{W\text{-}CeZr}$ = 0.66 g and $m_{W\text{-}ZrCe}$ = 0.33 g.

Significantly higher (up to 50%-units) H_2 conversions (X_{H_2}, %) were obtained on W-CeZr than W-ZrCe catalyst in the whole temperature range of 200–300 °C (Fig. 1). Hydrogen conversions over both catalysts were over 90% above 350 °C.

N_2-selectivity (S_{N_2}, %) and N_2O production (ppm) results obtained over the W-ZrCe and W-CeZr catalysts towards H_2-SCR are shown in Fig. 2. As already mentioned in Section 2.3, no ammonia was formed. Both W-CeZr and W-ZrCe catalysts show N_2-selectivities in the 70–92%-range for the wide temperature range of 200–450 °C, with the best selectivity obtained at 300 °C. Differences in N_2-selectivity between 5% and 10%-units are only observed at 200 and 400 °C. Due to the very low NO_x conversion obtained at 150 °C and 500–600 °C in the case of W-ZrCe, and at 150 °C and 550–600 °C in the case of W-CeZr catalyst, N_2-selectivites are not reported in Fig. 2 for these specific temperatures of 150, 550 and 600 °C. The N_2O concentration observed was practically below 15 ppm in the whole temperature range of 150–600 °C.

The NO and NO_2 concentrations in the gas effluent stream from the catalytic reactor for the W-ZrCe and W-CeZr catalysts as a function of reaction temperature are presented in Fig. 3a and b, respectively. The concentrations of NO recorded over the W-ZrCe and W-CeZr catalysts were lower than the NO_{in} values in the whole temperature range of 150–600 °C, with the lowest value achieved at 300 and 250 °C,

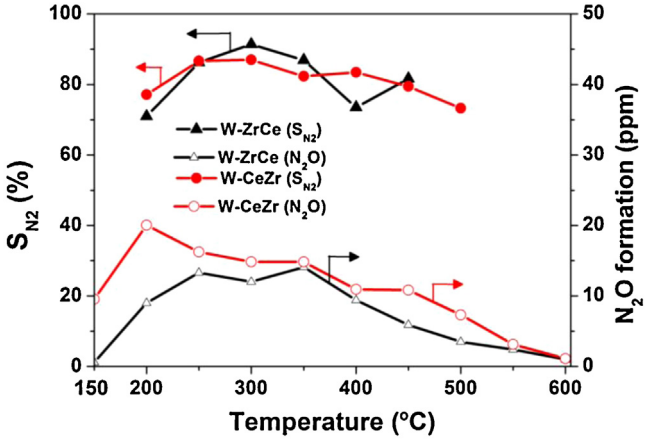

Fig. 2. N_2-selectivity (S_{N_2}) and N_2O formation (ppm) in the H_2-SCR as a function of temperature over W-ZrCe and W-CeZr catalysts. Reaction conditions: 520 ppm NO_x (NO:NO_2 ~9:1), 1.0 vol% H_2, 5 vol% O_2, 10 vol% CO_2 and He as balance gas; GHSV ~51,000 h^{-1}; $m_{W\text{-}CeZr}$ = 0.66 g and $m_{W\text{-}ZrCe}$ = 0.33 g.

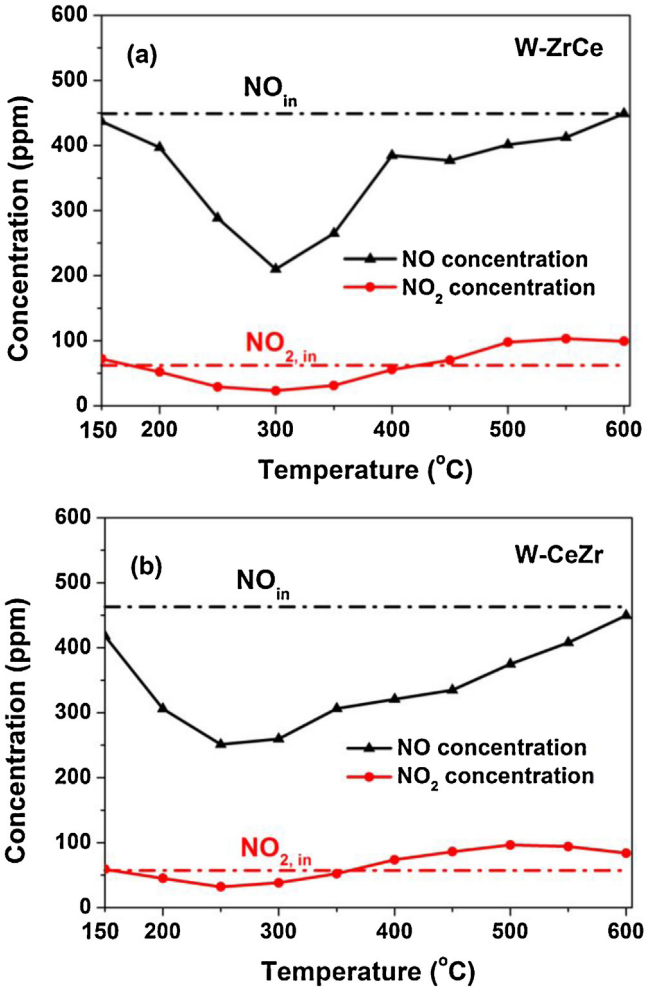

Fig. 3. NO and NO_2 concentrations at the outlet of the microreactor in the H_2-SCR as a function of temperature over W-ZrCe (a) and W-CeZr (b) catalysts. The inlet (feed) NO and NO_2 concentrations are also shown (dashed lines). Reaction conditions: 520 ppm NO_x (NO:NO_2 ~9:1), 1.0 vol% H_2, 5 vol% O_2, 10 vol% CO_2 and He as balance gas; GHSV ~51,000 h^{-1}; $m_{W\text{-}CeZr}$ = 0.66 g and $m_{W\text{-}ZrCe}$ = 0.33 g.

respectively. On the other hand, NO_2 concentrations were lower than $NO_{2,\ in}$ at 200–350 °C but higher above 450 °C over both W-CeZr and W-ZrCe catalysts. In the 250–350 °C range, the latter catalyst shows lower NO_2 concentrations than the former one indicating increased reduction rates by hydrogen or lower oxidation rates of NO by oxygen as will be discussed below.

Fig. 4 presents comparative results of the integral specific reaction rate of NO (R_{NO}, see Eq. (6)) expressed per m^2 of catalyst surface (μmol NO m^{-2} min^{-1}), and of the NO conversion (X_{NO}) as a function of reaction temperature. Based on these results, it is clearly illustrated that the W-ZrCe catalyst possesses either a larger concentration of active sites or sites of higher reactivity per m^2 than the W-CeZr solid. It is remarkable that in the case of W-ZrCe, R_{NO} values are larger in the whole temperature range of 200–500 °C. In particular, the maximum integral specific reaction rate estimated over the W-ZrCe solid at 300 °C is 0.14 μmol m^{-2} min^{-1}, which is three times higher than the corresponding value obtained over the W-CeZr catalyst at 250 °C. On the other hand, the maximum activity in terms of NO conversion over the W-ZrCe solid was about 10%-units higher only compared to the W-CeZr catalyst.

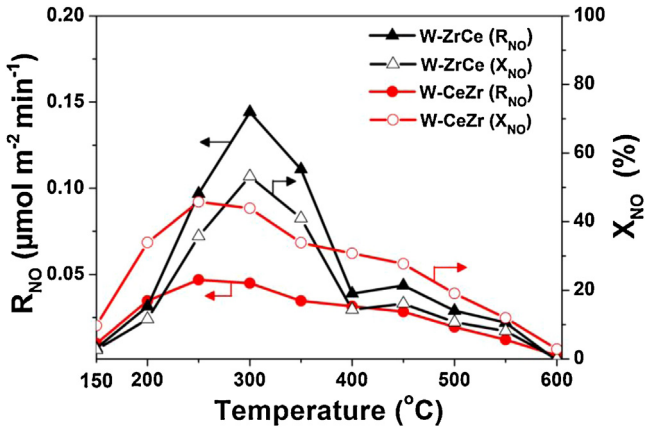

Fig. 4. Specific integral reaction rate of NO, R_{NO} (μmol NO m^{-2} min^{-1}) and NO conversion (X_{NO}, %) in the H_2-SCR as a function of temperature over W-ZrCe and W-CeZr catalysts. Reaction conditions: 520 ppm NO_x (NO:NO_2 ~9:1), 1.0 vol% H_2, 5 vol% O_2, 10 vol% CO_2 and He as balance gas; GHSV ~51,000 h^{-1}; $m_{W\text{-}CeZr}$ = 0.66 g and $m_{W\text{-}ZrCe}$ = 0.33 g.

3.1.2. *Effect of water on the X_{NO} (%) and S_{N_2} (%)*

The presence of about 7 vol% H_2O in the feed stream consisting of 520 ppm NO, 1% H_2, 5%O_2, 10% CO_2 (He balance) was investigated at 51,000 h^{-1} and at 250 and 300 °C over the W-ZrCe and W-CeZr catalysts. It was found that a drop in NO conversion by 10 and 15%-units was obtained at 250 and 300 °C, respectively over the W-ZrCe catalyst following a 30-h run. On the other hand, the N_2O selectivity dropped to 5–7% (250–300 °C) to be compared to the value of 10–12% obtained in the absence of water in the feed (Fig. 2). Similar results for the extent of decrease in both the X_{NO} (%) and S_{N_2O} (%) were also seen for the W-CeZr catalyst. No ammonia formation could be detected as in the case of the absence of water in the feed.

3.1.3. *Effect of H_2 and O_2 feed gas concentrations on W-CeZr catalyst performance*

Fig. 5a illustrates that the vol% of H_2 and O_2 in the reaction feed gas stream largely influences the NO_x conversion obtained on the W-CeZr catalyst. The highest NO_x conversion obtained was 46% at 250 °C with the reaction gas mixture containing 5% O_2 and 1% H_2. When the feed concentration of O_2 was doubled (10% O_2, 1% H_2), the maximum NO_x conversion was only 29% at 300 °C (Fig. 5a). At the same temperature, the NO_x conversion was 24% for the gas mixture containing 5% O_2 and 0.6% H_2. The N_2-selectivity behavior is reported in Fig. 5b. It is seen that when the H_2 feed concentration is reduced from 1.0 to 0.6% (O_2: 5 vol%) N_2-selectivity is significantly reduced at T > 300 °C, whereas the opposite behavior is observed when the O_2 feed concentration is increased from 5 to 10% (H_2: 1 vol%). On the other hand, the temperature at which maximum N_2-selectivity is observed remains the same (300 °C) for all three H_2:O_2 feed ratios. It is noted also that N_2O formation was lower than 20 ppm in all three feed gas compositions reported in Fig. 5, where in the case of 1% H_2–10% O_2 in the feed lower concentrations of N_2O were seen compared to the case of 0.6% H_2–5% O_2 feed composition. The latter result indicates that the presence of highly oxidized feed gas stream (e.g. 10% O_2) reduces the formation of N_2O over the W-CeZr catalyst.

3.1.4. *Stability test*

The stability of the W-CeZr catalyst with time on stream was examined at 250 °C (the T at which highest NO_x conversion was achieved) using a reaction feed gas stream consisting of 540 ppm NO_x (NO:NO_2 ~9:1), 1% H_2, 5% O_2, 10 vol% CO_2 and He balance gas for 66 h. Fig. 6 presents the results of this stability test in terms of

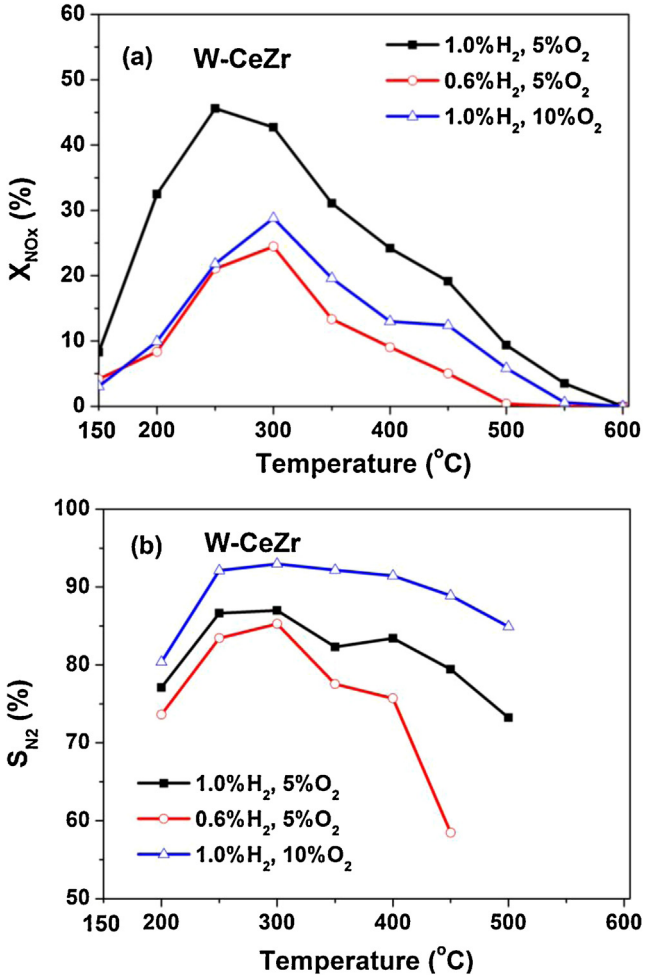

Fig. 5. The effect of H_2 and O_2 feed concentration on NO_x conversion (X_{NO_x}) (a) and N_2-selectivity (S_{N_2},%) (b) in the H_2-SCR as a function of temperature over the W-CeZr catalyst. Reaction conditions: 520 ppm NO_x (NO:NO_2 ~4:1; 10 vol% O_2 or NO:NO_2 ~9:1; 5 vol% O_2), 0.6–1.0 vol% H_2, 5–10 vol% O_2, 10 vol% CO_2, He balance gas; GHSV ~51,000 h^{-1}; $m_{W\text{-}CeZr}$ = 0.66 g and $m_{W\text{-}ZrCe}$ = 0.33 g.

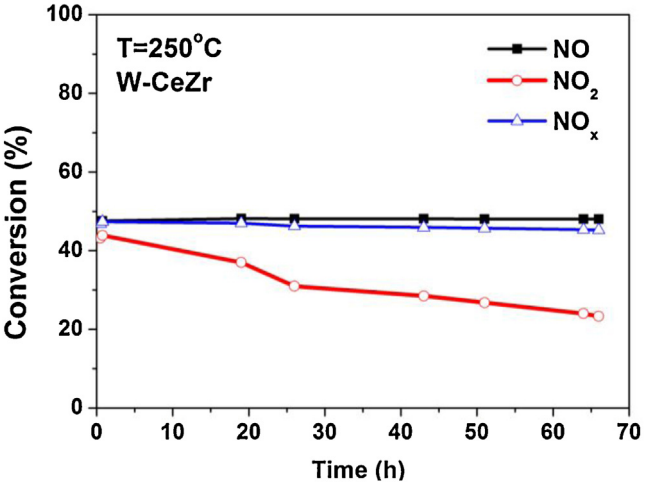

Fig. 6. Stability test (66 h) in the H_2-SCR of NO_x performed at 250 °C over the W-CeZr catalyst. Reaction conditions: 520 ppm NO_x (NO:NO_2 ~9:1), 1.0 vol% H_2, 5 vol% O_2, 10 vol% CO_2 and He as balance gas; GHSV ~51,000 h^{-1}; $m_{W\text{-}CeZr}$ = 0.66 g.

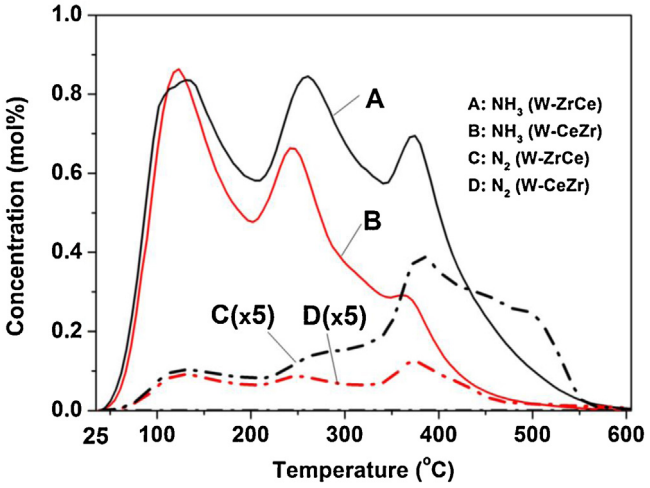

Fig. 7. NH_3 and N_2 desorption profiles obtained over W-ZrCe (A and C) and W-CeZr (B and D) catalysts during NH_3-TPD. NH_3 chemisorption conditions: 1.11%NH_3/He flow; T = 25 °C; F = 30 NmL min^{-1}, Δt = 30 min. TPD run in He flow: F_{He} = 30 NmL min^{-1}; β = 30 °C min^{-1}; W_{cat} = 0.3 g. N_2 desorption traces were multiplied by a factor of five (×5).

NO, NO_2 and NO_x conversions. The stability of the W-CeZr catalyst is good for the 66-h testing, since the NO conversion remained at 48% during the experiment, and the NO_x conversion followed also the same trend (only ~2% drop at the end of experiment). On the other hand, the individual NO_2 conversion decreased from 43 to 23% after 66 h on stream. Similar qualitative activity profiles for NO and NO_x were obtained on the W-ZrCe catalyst at 300 °C (T at which maximum X_{NO} (%) was achieved, see Fig. 1). In particular, the drop in the NO_x conversion was only 4% after 70 h on reaction stream.

3.1.5. *Effect of GHSV*

The effect of GHSV (h^{-1}) on the X_{NO} (%) and S_{N_2} (%) as a function of reaction temperature (250–400 °C) was investigated for the W-CeZr and W-ZrCe catalysts. For the former catalyst, the largest conversion of NO was 55% at 250 °C, whereas the lowest one 38% after using a GHSV of 10,000 h^{-1}. NO conversions approximately 8–10%-units lower were obtained using a GHSV of 51,000 h^{-1} compared to 10,000 h^{-1}. The effect of GHSV (10,000 vs. 51,000 h^{-1}) on the N_2-selectivity was found to be practically small (250–450 °C, 2–3%-units difference). In the case of W-ZrCe solid, a similar behaviour with respect to the X_{NO} (%) and S_{N_2} (%) was obtained after decreasing the GHSV from 51,000 to 10,000 h^{-1}.

3.2. *Catalyst characterization*

3.2.1. *Acidity measurements (Mass spectrometry NH_3-TPD and NH_3-DRIFTS)*

Fig. 7 shows NH_3 and N_2 desorption traces obtained during NH_3-TPD performed over the W-ZrCe and W-CeZr solids. In the case of W-ZrCe three major NH_3 desorption peaks were formed centered at T_M = 130, 260 and 375 °C, where W-CeZr also exhibits three major NH_3 desorption peaks (T_M = 123, 242 and 360 °C). Small amounts of N_2 and NO, and very small amounts (<0.2 μmol g^{-1}) of N_2O and NO_2 were detected during NH_3-TPDs in both solids. A broad N_2-TPD peak with shoulders and local maxima are observed over both the W-ZrCe and W-CeZr solids in the 70–560 °C and 70–480 °C ranges, respectively (Fig. 7C and D). Maximum N_2 desorption rate over both catalysts was achieved at ~375 °C. The N_2, NO and N_2O formation is due to the reaction of adsorbed NH_3-s

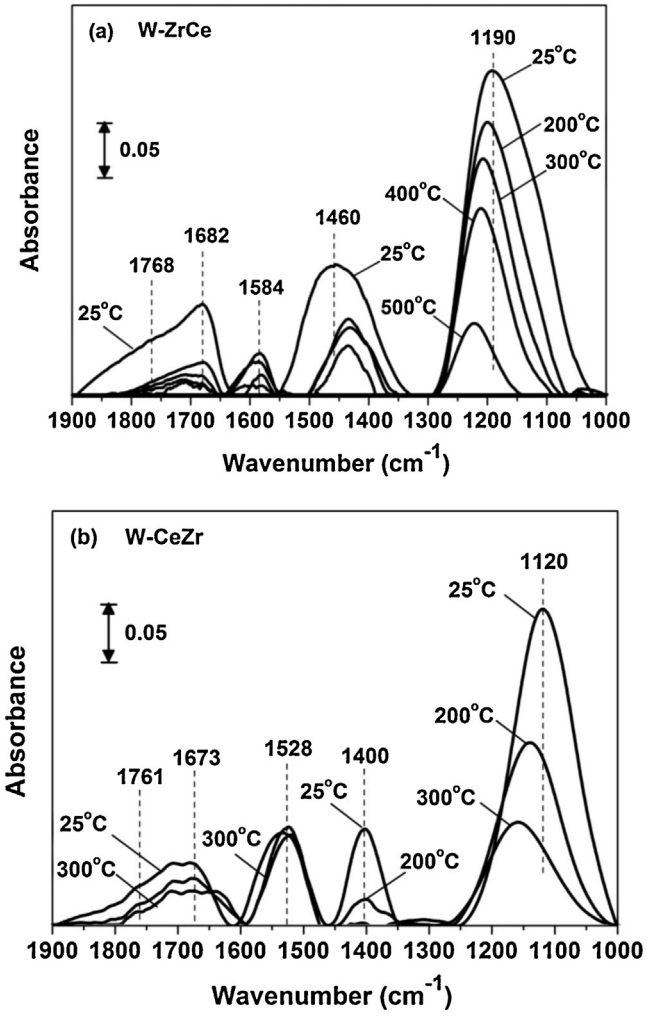

Fig. 8. In situ DRIFTS spectra recorded in the 1900–1000 cm^{-1} range after 0.55% NH_3/He chemisorption at 25 °C for 15 min followed by TPD in Ar flow over the W-ZrCe (a) and W-CeZr (b) catalysts.

with surface lattice oxygen (O_{L-s}). For example, in the case of N_2 formation the following reaction takes place:

$$2NH_{3-s} + 3O_{L-s} \rightarrow N_2(g) + 3H_2O(g) + 2s + 3[\square/e^-] - s \quad (7)$$

where [□/e^-]-s: surface oxygen vacant site. The NO_2 formation is rather due to the oxidation of NO by lattice oxygen. The amounts (μmol g^{-1}) of all desorbed gases obtained during TPDs are provided in Table 3. Numbers in parentheses for NH_3 desorption indicate the respective specific amounts estimated per m^2 of catalyst surface. It is seen that the concentration of acid sites is about twice as large for the W-ZrCe compared to W-CeZr solid (5.2 vs. 2.5 μmol m^{-2}).

Fig. 8a and b show in situ DRIFTS spectra in the 1000–1900 cm^{-1} range recorded on the W-ZrCe and W-CeZr catalysts, respectively, after NH_3 chemisorption (0.55% NH_3/He) at 25 °C followed by temperature-programmed desorption in Ar flow (TPD up to 600 °C). Three rather symmetrical IR bands and a non-symmetrical broad IR band (1900–1650 cm^{-1}) were observed. In the case of W-ZrCe (Fig. 8a), the IR bands located at 1584 and 1190 cm^{-1} correspond to the asymmetric and symmetric bending vibrational modes of N—H bond in NH_3 co-ordinately linked to Lewis acid sites [56–58]. The IR band at 1460 cm^{-1} corresponds to the asymmetric bending vibrational mode of NH_4^+ on Brönsted acid sites [56], whereas the broad IR band at 1682 cm^{-1} is attributed to the symmetric bending vibrational mode (N—H) in the NH_4^+, which is associated to Brönsted acid sites [59,60]. The stepwise increase in the catalyst

Table 3
Specific amounts (μmol g^{-1}) of desorbed species in NH_3-TPD, NO-TPD and H_2/O_2-TPSR experiments performed over W-ZrCe and W-CeZr catalysts.

Experiment	Catalyst	NH_3 (μmol g^{-1})	NO (μmol g^{-1})	N_2 (μmol g^{-1})	N_2O (μmol g^{-1})	NO_2 (μmol g^{-1})	Total (μmol g^{-1})
NH_3-TPD	W-ZrCe	346.9 (5.2)[a]	6.5	23.3	0.2	0.1	400.5 (5.96)[a]
	W-CeZr	229.2 (2.5)[a]	7.1	8.6	0.1	0.1	253.8 (2.76)[a]
NO-TPD	W-ZrCe	0.6	30.8 (0.46)[a]	0.1	0.2	1.2	33.2
	W-CeZr	0.3	23.5 (0.26)[a]	0.2	0.1	0.2	24.6
H_2/O_2-TPSR	W-ZrCe	1.2	118.7	3.7	1.1	46.4	175.9 (2.62)[a]
	W-CeZr	1.6	132.4	7.2	0.8	65.3	215.3 (2.34)[a]

[a] Estimated values (μmol m^{-2}) based on the BET surface area.

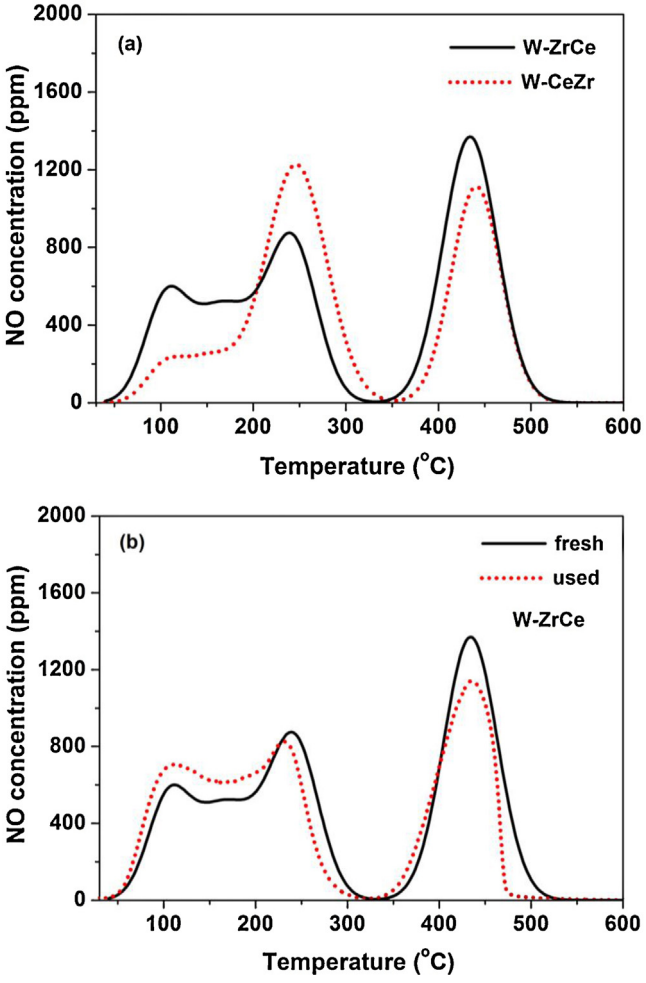

Fig. 9. NO-TPD traces obtained over (a) the fresh W-ZrCe and W-CeZr catalysts, and (b) over the used ($NO/H_2/O_2/CO_2/H_2O$/He; 30-h on stream) W-ZrCe catalyst. NO chemisorption: 0.1% NO/He (100 NmL min^{-1}), $T = 25\,^{\circ}C$; $\Delta t = 30$ min; TPD run: He flow (30 NmL min^{-1}); $\beta = 30\,^{\circ}C\,min^{-1}$; $W_{cat} = 0.3$ g.

temperature from 25 to 600 °C in Ar flow resulted in a clear progressive decrease in the integral IR band intensity associated with all the kinds of adsorbed NH_3 species. In the case of W-CeZr (Fig. 8b), the IR bands disappear completely at 400 °C, whereas in the case of W-ZrCe (Fig. 8a) the corresponding IR bands pertain up to 600 °C. It is therefore conclusive that NH_3 is more strongly adsorbed (thermally stable) on the W-ZrCe than the W-CeZr solid surface. The implications of this result on the catalytic performance of the two solids will be discussed later on.

3.2.2. NO-TPD

Temperature-programmed desorption traces of NO obtained over the fresh W-CeZr and W-ZrCe catalysts are shown in Fig. 9a. Three NO desorption peaks ($T_M = 114$, 243 and 445 °C) are observed in the case of W-ZrCe catalyst; the largest NO desorption peak was detected at 445 °C. In the case of W-CeZr catalyst, two NO desorption peaks were found at 245 and 445 °C with a large shoulder at the rising part of the 1st desorption peak (Fig. 9a). It was found that W-ZrCe adsorbs larger amounts of NO_x per gram basis (30.8 μmol g^{-1}) or per surface area of the solid (0.46 μmol m^{-2}) than the W-CeZr solid (23.5 μmol g^{-1} and 0.26 μmol m^{-2}). It is worth pointing out that no significant amounts of other gases (NH_3, N_2, NO_2 or N_2O) were formed during the NO-TPDs (Table 3).

NO-TPD was also performed on the W-ZrCe catalyst following H_2-SCR in the presence of H_2O in the feed stream (Section 2.3) for 30 h on reaction stream. Fig. 9b shows the result obtained, where for comparison, the NO-TPD of the fresh catalyst is also shown. It is seen that the presence of 7 vol% H_2O and 10% CO_2 in the H_2-SCR feed stream changed only slightly the adsorption/desorption behavior of NO. For example, the total amount of NO desorbed was 28.1 μmol g^{-1} to be compared to the value of 30.8 μmol g^{-1} obtained for the fresh catalyst, whereas the shape and peak positions were very similar in both cases (Fig. 9b).

3.2.3. H_2/O_2-Temperature programmed surface reaction studies

Fig. 10 presents NO and NO_2 (a) and N_2 (b) desorption traces obtained over the W-CeZr and W-ZrCe catalysts during H_2/O_2-TPSR (see Section 2.2.3). The NO desorption trace over the W-ZrCe catalyst presents two discernible peaks (139 and 374 °C) with shoulders on the rising and falling parts of the 2nd peak (Fig. 10a, curve A). In the case of the W-CeZr catalyst, three clearly discernible peaks are observed (130, 376 and 437 °C) with a shoulder on the rising part of the second NO peak. The total amount of NO desorption from the W-ZrCe catalyst was found to be lower by 24% compared to that on the W-CeZr solid. Furthermore, the 1st desorption peak of NO on the W-ZrCe is clearly larger than that observed on the W-CeZr solid (Fig. 10a, curves A and B). In addition, two clearly discernible NO_2 peaks are observed at 160 and 402 °C for the W-ZrCe solid and at 163 and 387 °C for the W-CeZr one with a shoulder at the rising part of the 2nd peak over both solids. The amount of NO_2 measured on the W-ZrCe solid was found to be lower by 30% compared to that on the W-CeZr solid (Table 3).

Fig. 10b shows TPSR traces of N_2 formation in the flow of 1% H_2/5% O_2/He gas mixture. In both catalysts two clearly discernible N_2 peaks were obtained, where a very small third peak can also be seen in the case of the W-ZrCe starting at ~500 °C and extending out to 600 °C (Fig. 10b). The W-CeZr solid exhibits N_2 peaks at 88 and 342 °C, whereas the W-ZrCe one at 117 and 346 °C. The total amount (μmol g^{-1}) of N_2 formation on both solids is reported in Table 3, where the W-CeZr solid exhibits about twice as much N_2 desorption than the W-ZrCe one. On the basis of Fig. 10b, W-CeZr shows larger amounts of produced N_2 than the W-ZrCe one in the 50–200 °C range but similar quantities in the 300–450 °C range. The significance of these results and their relationship with catalysts' activity behavior (Fig. 1) will be discussed in the following Section 4. It is worth pointing out that H_2 was almost completely consumed at temperatures above 480 and 460 °C (not presented) for the W-ZrCe and W-CeZr catalysts, respectively. No significant amounts of NH_3 and N_2O were found to desorb during the H_2/O_2-TPSR (Table 3).

3.2.4. UV–vis/DRS studies

Fig. 11 presents in situ UV–vis/DR spectra recorded on CeZr, ZrCe, W-CeZr and W-ZrCe solids (see Section 2.2.5). In the case of CeZr solid (Fig. 11d), two absorption bands were recorded at 280 (not shown) and 315 nm due to charge transfer from the O 2p to the Ce^{4+} 4f orbital, and to inter-band transitions, respectively [61]. The spectrum of the W-CeZr catalyst (Fig. 11b) exhibits further absorption bands at 300 and 348 nm which correspond to polymeric WO_6 and WO_3, respectively [62]. Gutierrez-Alejandre et al. [63] and Maia et al. [64] reported that ZrO_2 exhibits only one absorption band at 210 nm with a tail in the 250–400 nm region. This behaviour is similar to the one observed in the present ZrCe solid (Fig. 11c). The W-ZrCe exhibits further absorption at 300 nm (not shown in the y-scale of Fig. 11) due to WO_6. The higher intensities observed in the W-CeZr and W-ZrCe catalysts compared to the corresponding ones of supports alone is due to the overlapping of the respective bands due to the support (CeZr or ZrCe) and tungsten oxide.

The plot of square root of Kubelka–Munk function multiplied by the photon energy ($[F(R_\infty)h\nu]^2$) against the photon energy ($h\nu$, eV) was used to determine the energy band gap (see Fig. 11, inset) of the W-ZrCe and W-CeZr solids. The energy band gap values

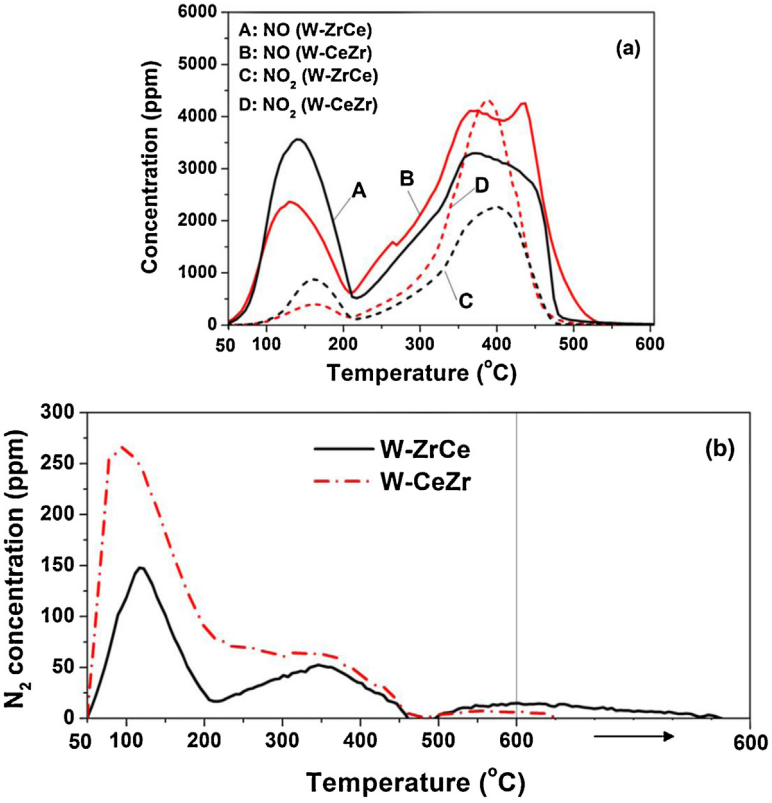

Fig. 10. (a) NO and NO_2 desorption traces obtained over W-ZrCe (A and C) and W-CeZr (B and D) catalysts in H_2/O_2-TPSR. (b) N_2 desorption traces obtained over W-ZrCe and W-CeZr catalysts in H_2/O_2-TPSR. NO chemisorption conditions: 0.1% NO/10% O_2/He (100 NmL min^{-1}); T = 25 °C; Δt = 30 min. TPSR run: 1% H_2/5% O_2/He flow (30 NmL min^{-1}), β = 30 °C min^{-1}; W_{cat} = 0.3 g.

were obtained by extrapolating the linear part of the rising part of the curve to zero [52,53,65]. According to the literature [63,64,66], CeO_2, ZrO_2 and WO_3 have an energy band gap of 3.1, 5.0 and 2.8 eV, respectively. The CeZr and ZrCe solids provided an energy band gap of 3.10 and 3.70 eV, respectively. The energy band gap of ZrCe was found to be lower than that of ZrO_2 and higher than that of CeO_2, indicating the effect of Zr^{4+} doping on the electronic states of CeO_2. The energy band gaps of the W-CeZr and W-ZrCe were found to be 3.10 and 3.65 eV, respectively. In the case of W-ZrCe, the energy band gap was slightly decreased with respect to that of support alone, indicating that some electronic modifications occurred when WO_x was deposited on ZrCe. On the contrary, no effect was noticed when WO_x was deposited on CeZr.

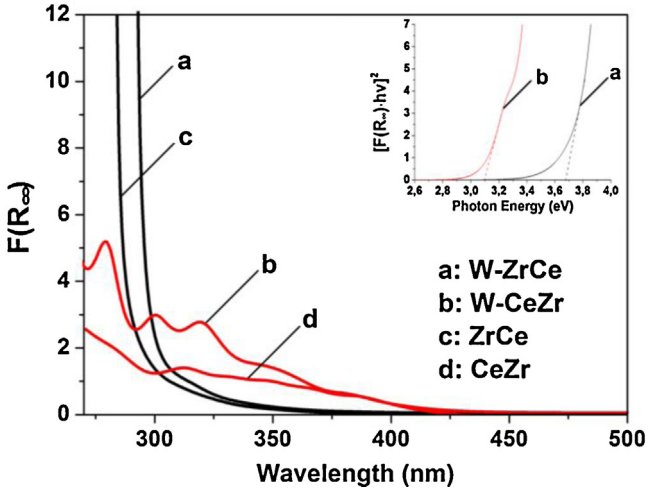

Fig. 11. UV–vis/DR spectra and energy band gaps estimation (eV, inset graph) obtained over ZrCe, CeZr, W-ZrCe and W-CeZr solids. Fresh samples were pretreated in Ar flow (60 NmL min^{-1}) at 150 °C for 1 h before spectra were recorded at 25 °C in Ar flow.

4. Discussion

In order to better understand the H_2-SCR of NO_x on the present W-CeZr and W-ZrCe metal oxide surfaces, fundamental mechanistic information must first be provided and discussed in order to correctly relate the observed catalytic activity of the solids with some of their important surface physico-chemical properties elucidated in the present work. The following discussion is appropriate:

(i) Hydrogen chemisorption was reported to occur on metal oxide surfaces via heterolytic splitting onto an adjacent *metal cation* (s1) and *oxygen anion* (s2) pair site in the 100–500 °C range [67]:

$$H_2(g) + s1 + s2 \rightarrow H\text{-}s1 + H\text{-}s2 \quad (8)$$

where H on site s1 is then transferred to an adjacent s2 site.

(ii) Oxygen chemisorption occurs on oxygen vacant sites (s3) according to the following elementary step [36,67]:

$$O_2(g) + 2\,s3 \leftrightarrow 2O\text{-}s3 \quad (9)$$

(iii) Formation of water occurs via a hydroxyl (–OH) intermediate species [67–69]:

$$H\text{-}s1(\text{or } H\text{-}s2) + O\text{-}s3 \rightarrow OH\text{-}s1(\text{or } OH\text{-}s2) + s3 \quad (10)$$

$$OH\text{-}s1(\text{or } OH\text{-}s2) + H\text{-}s2(\text{or } H\text{-}s1) \rightarrow H_2O(g) + s1(\text{or } s2) + s2(\text{or } s1) \quad (11)$$

(iv) Interaction of NO/NO_2 with metal oxide surfaces can lead to a number of nitrite (NO_2^-), nitrate (NO_3^-) and nitrosyl ($NO^{\delta+}$) species, where their concentration strongly depends on the chemical composition of the metal oxide, the concentration of NO, NO_2 and O_2 in the feed gas stream, and the reaction temperature [13,32–34,70]. Reduction of the thus formed adsorbed NO_x species occurs via sequential addition of H-s2 (or H-s1) species. For example:

$$2NO\text{-}s2 + 4H\text{-}s2 \rightarrow N_2(g) + 2H_2O(g) + 6s2 \quad (12)$$

$$2NO\text{-}s2 + 2H\text{-}s2 \rightarrow N_2O(g) + H_2O(g) + 4s2 \quad (13)$$

The chemical steps (12) and (13) are not considered as true elementary reaction steps since other intermediates between the NO-s2 precursor and the final $N_2(g)$ or $N_2O(g)$ gas products are not detailed here (e.g. NH_x-s2 intermediates).

(v) Chemisorption of $CO_2(g)$ on metal oxide surfaces occurs via both oxygen anion (s2) and oxygen vacant sites (s3) leading to the formation of various types of carbonate species [71,72].

Based on the above fundamental considerations regarding the interactions between H_2, O_2, NO/NO_2 and CO_2 gases (found in the present H_2-SCR feed gas composition) with the present solid surfaces, the volcano-type behavior shown in Figs. 1 and 4 can be better explained. Along these lines, the nature and concentration of active NO_x formed on the two catalytic surfaces, the competitive kinetics of O_2 (5 vol%) and CO_2 (10 vol%) chemisorption on the same sites (s3), and the competitive chemisorption of NO/NO_2 and H_2 on sites s1 (metal cation) and s2 (oxygen anion) must also be considered.

As illustrated in Fig. 10 and Table 3, adsorbed NO_x species formed on the W-CeZr and W-ZrCe surfaces after the NO/O_2/He gas treatment at 25 °C decomposed into NO and NO_2 but reacted also towards N_2 gas in different amounts ($\mu mol\ g^{-1}$) at a given temperature range (ΔT). For example, at $T < 200$ °C less NO_x (NO and NO_2) is formed on the W-CeZr catalyst in harmony with the higher NO_x conversion and specific integral rate obtained compared to the case of the W-ZrCe solid (Figs. 1 and 4). On the other hand, the opposite is true for the temperature range of $200 < T < 350$ °C, where less NO_x is formed on W-ZrCe, in harmony with the larger NO_x conversion and specific integral rate obtained compared to the case of W-CeZr. Therefore, the concentration of adsorbed NO_x and their thermal stability under H_2/O_2 gas atmosphere, as well as the rate of hydrogen combustion (steps (8)–(11)) are important kinetic parameters that eventually determine the NO_x conversion and specific integral rate behavior with reaction temperature. It was reported [67] that hydrogen combustion is facilitated on reducible metal oxides. This result is in harmony with the hydrogen conversion vs. T profiles (Fig. 1), where the W-CeZr (Ce-rich) is expected to have a higher concentration of oxygen vacant sites than the W-ZrCe (Zr-rich) solid [36,73], in accordance also with the XRD results (t-ZrO_2 was formed). The formation of NO and NO_2 during the H_2/O_2-TPSR experiment (Fig. 10a) illustrates that most of adsorbed NO_x are not able to react with hydrogen towards N_2 and N_2O, and these species must be considered as inactive (or spectator) species of the H_2-SCR. A large concentration of inactive NO_x was also formed on the MgO and CeO_2 carriers over Pt/MgO-CeO_2 in the case of H_2-SCR [29,30,32–34].

The N_2-TPSR traces reported in Fig. 10b are very important since they suggest that at least two kinds of active NO_x are formed on W-CeZr and W-ZrCe catalysts (after 0.1%NO/10%O_2/He gas treatment at 25 °C), which then selectively react with H_2 to form N_2 in the presence of oxygen (1% H_2/5% O_2/He) under similar conditions as in the H_2-SCR. The amount ($\mu mol\ g^{-1}$) of the low-temperature N_2 trace (50–200 °C) for the W-CeZr is more than twice that obtained on the W-ZrCe catalyst, whereas that found in the 250–450 °C range is similar. These results provide support to the activity results shown in Fig. 1, where large differences in NO_x conversion can be seen at $T < 350$ °C but small differences at $T > 350$ °C (after considering the fact that twice as much amount of W-CeZr than of W-ZrCe was used).

A similar volcano-type behavior observed in the H_2-SCR on supported noble (Pt, Pd) metal catalysts [11–13,15,29,30,34,74,75] was explained as due to (a) the hydrogen combustion reaction (X_{H_2} vs. T), (b) the oxidation of noble metal, which reduces its ability to dissociate molecular hydrogen (active reducing species), and (c) the formation of different kinds of active NO_x (different reactivity) with reaction temperature [34]. The fact that NO_2 could have also been considered as a key intermediate of H_2-SCR (derived from the oxidation of NO), where its rate of formation is kinetically limited at low-temperatures, may not be excluded [76]. In the present case of H_2-SCR on the W-CeZr and W-ZrCe metal oxide surfaces, hydrogen combustion may partly explain the observed volcano-type activity behavior shown in Figs. 1 and 4. At 250 °C, where maximum X_{NO} or specific integral reaction rate does occur on W-CeZr (Fig. 4), the X_{H_2} is 53% (Fig. 1). On the other hand, at the same temperature the specific integral reaction rate on W-ZrCe increases by a factor of two, whereas the X_{H_2} is only 13%.

By comparing the NO and NO_2 effluent concentration profiles given in Fig. 3, it is clear that in the 300–350 °C range NO and NO_2 conversions are higher over the W-ZrCe than W-CeZr solid as also depicted in Fig. 1 (consider also the double amount of W-CeZr used compared to W-ZrCe). It is likely that in this temperature range the kinetics of reduction of NO_2 by H_2 is favored over the W-ZrCe than W-CeZr catalyst. This is related to the H_2-O_2/TPSR results (Fig. 10), where in the high temperature range of 300–450 °C significantly less NO_2 but similar amounts of N_2 are formed in the case of W-ZrCe catalyst.

The specific integral reaction rate of NO conversion ($\mu mol\ NO\ m^{-2}\ min^{-1}$) vs. T profile (Fig. 4) reveal that the W-ZrCe is by far more active in the 250–400 °C range, showing also a slightly better activity in the 400–600 °C range compared to the W-CeZr solid. This result suggests that very likely the specific concentration of active NO_x ($\mu mol\ NO_x\ m^{-2}$) is higher on the W-ZrCe than on the W-CeZr solid, and/or the former solid possesses NO_x adsorption sites (per m^2) of *higher site reactivity* towards H_2-SCR than the W-CeZr solid. On the basis of the H_2-O_2/TPSR results reported in Table 3, the W-ZrCe solid possesses about 12% higher concentration of total NO_x ($\mu mol\ m^{-2}$) (formed under 0.1%NO/10%O_2/He gas treatment) compared to W-CeZr. However, the true concentration of active NO_x present under H_2-SCR can only be verified via SSITKA-MS studies [32–34], subject out of the scope of this work. The implication of the results shown in Fig. 4 is that the preparation of W-ZrCe solid having an increased S_{BET} ($m^2\ g^{-1}$) will result in even higher NO_x conversions compared to those obtained in the W-CeZr solid (Figs. 1 and 4) given that the same site reactivity (k, s^{-1}) is obtained.

The N_2-selectivity behavior of the two solids in the 200–450 °C range (Fig. 2) is similar with only small differences (no more than 10%-units). In addition, W-CeZr shows very good N_2-selectivity values (77–87%) in a wide temperature range (200–450 °C) comparable to many active and selective noble metal supported catalysts [11–13,74,75]. By boosting the NO_x reduction activity (H_2-SCR) of the W-ZrCe solid to values larger than 80%, and keeping the N_2-selectivity in similar values to those found in the present work, these materials could be seen as potential catalysts towards H_2-SCR applications. As previously mentioned, W-ZrCe of higher BET area but also the modification of its chemical composition could result in the boosting of its H_2-SCR activity. The effect of water (7 vol%) in the feed stream on the performance of the W-ZrCe catalyst was found to be detrimental (10–15%-units drop at 250–300 °C) but

not severe. However, significantly longer times on stream (larger than 30 h of testing) must be investigated for practical applications.

In the case of use of the H_2-SCR of NO_x in stationary applications [16,28], the economics of the process would be favorable if lower H_2 feed concentrations are used. In the case where 5 vol% O_2 was present in the H_2-SCR feed composition (typical average oxygen composition in industrial flue gases), a decrease in the H_2 feed content from 1.0 to 0.6 vol% resulted in a significant drop in the NO_x conversion in the 150–300 °C range but no more than 18%-units at the high-T range of 350–500 °C in the case of the W-CeZr catalyst (Fig. 5a). It is obvious that the kinetics of NO_x reduction has a positive order with respect to hydrogen which varies in the 150–600 °C range. A similar result was also reported in the case of supported Pt catalysts [11,12]. In the case when the O_2 feed composition increased from 5 to 10 vol%, a similar effect on the NO_x conversion was seen as with the H_2 feed composition drop (from 1.0 to 0.6 vol%) at the low-T range of 150–300 °C. However, at the high-T range of 350–500 °C, the effect was smaller (less than 10%-units drop, see Fig. 5a).

The traces of NO, NO_2 and N_2 in the H_2/O_2-TPSR (Fig. 10a) suggest that very likely at least three kinds of different adsorbed NO_x species are formed during H_2-SCR, the concentration of which depends strongly on the catalyst composition (W-CeZr vs. W-ZrCe). On the basis of the NO-TPD (Fig. 9) and H_2/O_2-TPSR (Fig. 10) results, the concentration of adsorbed NO_x appears to be influenced by the presence of O_2 in the NO adsorption gas (see Table 3). A higher concentration of adsorbed NO_x was formed when 10% O_2 was present in the 0.1% NO/He adsorption gas mixture for both catalysts (Table 3), in harmony with previous studies [77,78].

The stability of the W-CeZr catalyst tested for 66 h of continuous H_2-SCR at 250 °C was excellent in terms of NO conversion. However, some drop in the activity of the catalyst after about 20 h on stream was observed in terms of NO_2 conversion (Fig. 6). This behavior could be interpreted as due to either a reduced rate of NO_2 reduction by hydrogen or to a progressive formation of some NO_2. Both interpretations might be considered since the ability of the catalyst to form NO_2 is rather clear at $T > 350$ °C (Fig. 3). The NO_2 formation is considered to take place via oxidation of NO by surface labile lattice oxygen. It is speculated whether the available concentration of this labile oxygen decreases with time on stream due to the competitive chemisorption of CO_2 (10 vol% present in the feed stream) to form stable carbonates (250 °C).

According to the NH_3-TPD (Fig. 7, Table 3) and NH_3-DRIFTS (Fig. 8) results, it is seen that W-CeZr and W-ZrCe solids present large differences in the concentration and strength of surface acid sites. Lewis acid sites are offered for NO_x formation upon NO interaction with the present metal oxide surfaces via the formation of nitrosyl species (M-$NO^{\delta+}$; M: Ce^{4+}, Zr^{4+} and W^{6+}). Costa and Efstathiou [32,33] have illustrated via SSITKA-DRIFTS studies that Ce-$NO^{\delta+}$ adjacent to a nitrate species formed on CeO_2 at the Pt-ceria interface is an active intermediate in the H_2-SCR on the Pt/CeO_2-MgO. It is therefore expected that the *concentration* (mol m^{-2}) and quality of the acid sites on the present W-CeZr and W-ZrCe surfaces, including those from the WO_x supported phase, must play a role on the formation of active NO_x in the H_2-SCR. The W-ZrCe solid was found to possess about twice as much acid sites per m^2 (measured by ammonia chemisorption) than the W-CeZr solid, and at the same time stronger Lewis acid sites (Fig. 8). It is speculated whether this result should be correlated with the higher specific activity (μmol m^{-2} min^{-1}) exhibited by the W-ZrCe compared to W-CeZr solid (Fig. 4). It is mentioned here that strong acid sites created on a sulfated zirconia support of Pt (Pt/s-ZrO_2) significantly improved the H_2-SCR activity at 100 °C and the N_2-selctivity in the 100–250 °C range [79]. Given the fact that the bonding of nitrosyl species on a Lewis acid site (L) occurs through the N-atom (L–$NO^{\delta+}$), then the strengthening of the L—N bond would result in the weakening of the N—O bond, thus facilitating the formation of N_2 or N_2O via the interaction with an adjacent NO_x species.

The fact that the chemical state of W in the W-CeZr and W-ZrCe catalysts is different, as revealed by the UV–vis/DRS studies (Fig. 11), it might be reasonable to also suggest that W oxidation state and local chemical environment (WO_x clusters) play a role on NO_x formation, as found in the NH_3-SCR on W-promoted MnO_x-CeO_2-ZrO_2 solids [80]. Furthermore, electronic interactions between WO_x and Pt were found to be responsible for the high low-T activity observed in the H_2-SCR of NO on the Pt/WO_3-ZrO_2 catalyst [81].

5. Conclusions

The following conclusions can be derived from the results of the present work.

(i) The catalytic activity of W-promoted Ce-Zr-O (Ce-rich or Zr-rich) solids towards H_2-SCR of NO_x was investigated for the first time. In the 250–350 °C range and at the GHSV of 51,000 h^{-1}, NO_x conversions in the 30–55%-range with N_2-selectivities in the 85–92%-range were noticed. A good stability in the activity of both W-ZrCe and W-CeZr catalysts is obtained at 300 or 250 °C, respectively, after 66 h on reaction stream ($NO_x/H_2/O_2/CO_2$/He). The presence of about 7 vol% H_2O in the feed stream resulted in a 10–15%-units drop in X_{NO} in the 250–300 °C range, but an improvement in N_2-selectivity by about 5%-units.

(ii) The specific integral reaction rate (μmol NO m^{-2} min^{-1}) of the W-ZrCe (Zr-rich) towards H_2-SCR in the 250–350 °C range was found to be 2–3 times higher than that on the W-CeZr (Ce-rich) solid. The preparation of W-ZrCe solids with higher S_{BET} (m^2 g^{-1}) is expected to boost the NO_x conversion values obtained on this solid for practical applications if the site reactivity remains the same.

(iii) At least two different kinds of adsorbed active NO_x species were identified on the W-CeZr and W-ZrCe catalysts that lead to the N_2 formation during H_2-SCR, the concentration of which is relatively small (4–7 μmol g^{-1}). Significantly larger amounts (>160 μmol g^{-1}) of other adsorbed NO_x which do not react with hydrogen (inactive or spectator species) are also formed.

(iv) Large differences in the total concentration and strength of surface acid sites, and in the concentration (μmol m^{-2}) of NO_x adsorption sites were identified among the W-CeZr and W-ZrCe solids (NH_3-TPD, NO-TPD and H_2/O_2-TPSR), factors that influence the catalytic behavior of these solids in the H_2-SCR of NO_x.

(v) In the case of the W-CeZr (Ce-rich) catalyst, the N_2-selectivity of the H_2-SCR was found to increase by 5–10%-units after increasing the O_2 feed concentration from 5 to 10 vol% in the 200–500 °C range, while an opposite behavior was obtained with the NO_x conversion. By decreasing the H_2 feed concentration from 1.0 to 0.6 vol%, NO_x conversion was reduced significantly at 200 and 250 °C (by ~25%-units), and to a lesser extent in the 300–500 °C range. On the other hand, the N_2-selctivity was slightly reduced in the 200–350 °C range (~5%-units) but to a larger extent at higher temperatures (e.g. ~20%-units at 450 °C).

Acknowledgements

The authors gratefully acknowledge the financial support from Tekes, the Finnish Funding Agency for Technology and Innovation via the Cleen Ltd's Future Combustion Engine Power Plant

(FCEP) programme, and the Research Committee of the University of Cyprus.

References

[1] Directives 98/69/EC, 2002/80/EC and 715/2007/EC of the European Parliament and Council.
[2] A. Väliheikki, T. Kolli, M. Huuhtanen, T. Maunula, T. Kinnunen, R.L. Keiski, Top. Catal. 56 (2013) 602–610.
[3] H. Chang, J. Li, J. Yuan, L. Chen, Y. Dai, H. Arandiyan, J. Xu, J. Hao, Catal. Today 201 (2013) 139–144.
[4] Z. Ma, D. Weng, X. Wu, Z. Si, J. Environ. Sci. 24 (2012) 1305–1316.
[5] P. Granger, V.I. Parvulescu, Chem. Rev. 111 (2011) 3155–3207.
[6] Y. Peng, K. Li, J. Li, Appl. Catal. B: Environ. 140–141 (2013) 483–492.
[7] M. Huuhtanen, T. Kolli, T. Maunula, R.L. Keiski, Catal. Today 75 (2002) 379–384.
[8] R. Burch, A. Ramli, Appl. Catal. B: Environ. 15 (1998) 49–62.
[9] M. Huuhtanen, Ph.D Thesis, University of Oulu, Finland, 2006.
[10] A. Łamacz, A. Krztoń, G. Djéga-Mariadassou, Appl. Catal. B: Environ. 142–143 (2013) 268–277.
[11] C.N. Costa, A.M. Efstathiou, Appl. Catal. B: Environ. 72 (2007) 240–252.
[12] C.N. Costa, P.G. Savva, J.L.G. Fierro, A.M. Efstathiou, Appl. Catal. B: Environ. 75 (2007) 147–156.
[13] G.G. Olympiou, A.M. Efstathiou, Chem. Eng. J. 170 (2011) 424–432.
[14] S. Yang, X. Wang, W. Chu, Z. Song, S. Zhao, Appl. Catal. B: Environ. 107 (2011) 380–385.
[15] Z. Liu, J. Li, I. Woo, Energy Environ. Sci. 5 (2012) 8799–8814.
[16] K. Polychronopoulou, A.M. Efstathiou, Recent Patents Mater. Sci. 5 (2012) 87–104.
[17] P. Forzatti, Appl. Catal. A: Gen. 222 (2001) 221–236.
[18] A.M. Efstathiou, K. Fliatoura, Appl. Catal. B: Environ. 6 (1995) 35–59.
[19] A. Fritz, V. Pitchon, Appl. Catal. B: Environ. 13 (1997) 1–25.
[20] V.I. Pârvulescu, P. Grange, B. Delmon, Catal. Today 46 (1998) 233–316.
[21] Z. Liu, S.-I. Woo, Catal. Rev. 48 (2006) 43–89.
[22] F.J. Janssen, in: G. Ertl, H. Knözinger, J. Weitkamp (Eds.), Handbook of Heterogeneous Catalysis, VCH, Weinheim, 1997, p. 1633.
[23] H. Gutberlet, B. Schallert, Catal. Today 16 (1993) 207–235.
[24] E. Kondratenko, V.A. Kondratenko, M. Richter, R. Fricke, J. Catal. 239 (2006) 23–33.
[25] K. Shimizu, A. Satsuma, Appl. Catal. B: Environ. 77 (2007) 202–205.
[26] D.E. Doronkin, S. Fogel, S. Tamm, L. Olsson, T. Khan, T. Bligaard, P. Gabrielsson, S. Dahl, Appl. Catal. B: Environ. 113–114 (2012) 228–236.
[27] S. Tamm, S. Fogel, P. Gabrielsson, M. Skoglundh, L. Olsson, Appl. Catal. B: Environ. 136–137 (2013) 168–176.
[28] A.M. Efstathiou, P.G., Savva, C.N. Costa, US 8,114,369 B2, 2012 (and references therein).
[29] C.N. Costa, V.N. Stathopoulos, V.C. Belessi, A.M. Efstathiou, J. Catal. 197 (2001) 350–364.
[30] C.N. Costa, P.G. Savva, Ch. Andronikou, P.G. Lambrou, K. Polychronopoulou, V.C. Belessi, V.N. Stathopoulos, P.J. Pomonis, A.M. Efstathiou, J. Catal. 209 (2002) 456–471.
[31] Q. Yu, F. Kong, L. Li, G. Wu, N. Guan, Chin. J. Catal. 31 (2010) 261–263.
[32] C.N. Costa, A.M. Efstathiou, J. Phys. Chem. B 108 (2004) 2620–2630.
[33] C.N. Costa, A.M. Efstathiou, J. Phys. Chem. C 111 (2007) 3010–3020.
[34] P.G. Savva, A.M. Efstathiou, J. Catal. 257 (2008) 324–333.
[35] P.G. Savva, C.N. Costa, A.M. Efstathiou, Kinet. Catal. 49 (2008) 743–747.
[36] A.M. Efstathiou, S.Y. Christou, Catalysis by Ceria and Related Materials, in: A. Trovarelli, P. Fornasiero (Eds.), Catalysis Science Series, Vol. 12, 2nd Ed., Imperial College Press, 2013, pp. 139–221, Ch. 3.
[37] M. Adamowska, S. Muller, P. Da Costa, A. Krzton, P. Burg, Appl. Catal. B: Environ. 74 (2007) 278–289.
[38] L. Chen, D. Wenga, Z. Si, X. Wu, Prog. Nat. Sci.: Mater. Int. 22 (2012) 265–272.
[39] M. Daturi, E. Finocchio, C. Binet, J.C. Lavalley, F. Fally, V. Perrichon, J. Phys. Chem. B 103 (1999) 4884–4891.
[40] M. Daturi, N. Bion, J. Saussey, J.-C. Lavalley, C. Hedouin, T. Seguelong, G. Blanchard, Phys. Chem. Chem. Phys. 3 (2001) 252–255.
[41] R. Zhang, W.Y. Teoh, R. Amal, B. Chen, S. Kaliaguine, J. Catal. 272 (2010) 210–219.
[42] M. Daturi, E. Finocchio, C. Binet, J.-C. Lavalley, F. Fally, V. Perrichon, H. Vidal, N. Hickey, J. Kaspar, J. Phys. Chem. B 104 (2000) 9186–9194.
[43] Z. Wang, Z. Qu, X. Quan, H. Wang, Appl. Catal. A: Gen. 411–412 (2012) 131–138.
[44] H. Vidal, J. Kašpar, M. Pijolat, G. Colonb, S. Bernal, A. Cordón, V. Perrichon, F. Fally, Appl. Catal. B: Environ. 27 (2000) 49–63.
[45] I. Atribak, N. Guillén-Hurtado, A. Bueno-López, A. García-García, Appl. Surf. Sci. 256 (2010) 7706–7712.
[46] G. Jing, J. Li, D. Yang, J. Hao, Appl. Catal. B: Environ. 91 (2009) 123–134.
[47] Y. Li, H. Cheng, D. Li, Y. Qin, Y. Xie, S. Wang, Chem. Commun. (2008) 1470–1472.
[48] A. Väliheikki, T., Kolli, M., Huuhtanen, T., Maunula, T., Kinnunen, R.L. Keiski, Conference Paper in East Meets West on Innovation and Entrepreneurship 2012, Conference Proceedings 327–334, ISBN: 978-9963-700-57-8.
[49] M.-C. Wang, H.-J. Huang, Thermochim. Acta 567 (2013) 93–99.
[50] J.W. Niemantsverdriet, in: Spectroscopy in Catalysis: An Introduction, 3rd Ed., Wiley, 2007.
[51] C.N. Costa, T. Anastasiadou, A.M. Efstathiou, J. Catal. 194 (2000) 250–265.
[52] K.C. Petallidou, A.M. Efstathiou, Appl. Catal. B: Environ. 140–141 (2013) 333–347.
[53] D.G. Barton, M. Shtein, R.D. Wilson, S.L. Soled, E. Iglesia, J. Phys. Chem. B 103 (1999) 630–640.
[54] C.D. Baertsch, S.L. Soled, E. Iglesia, J. Phys. Chem. B 105 (2001) 1320–1330.
[55] C. Perego, S. Peratello, Catal. Today 52 (1999) 133–145.
[56] T. Gu, R. Jin, Y. Liu, H. Liu, X. Weng, Z. Wu, Appl. Catal. B: Environ. 129 (2013) 30–38.
[57] W.S. Kijlstra, D.S. Brands, E.K. Poels, A. Bliek, J. Catal. 171 (1997) 208–218.
[58] L. Chen, J.H. Li, M.F. Ge, Environ. Sci. Technol. 44 (2010) 9590–9596.
[59] L. Chen, J. Li, M. Ge, Chem. Eng. J. 170 (2011) 531–537.
[60] L. Chen, J.H. Li, M.F. Ge, J. Phys. Chem. C 113 (2009) 21177–21184.
[61] K. Krishna, A. Bueno-Lopez, M. Makkee, J.A. Moulijn, Appl. Catal. B: Environ. 75 (2007) 210–220.
[62] Q. Zhu, X. Chu, Z. Zhang, W.-L. Dai, K. Fan, Appl. Catal. A: Gen. 435–436 (2012) 141–147.
[63] A. Gutierrez-Alejandre, J. Ramirez, G. Busca, Catal. Lett. 56 (1998) 29–33.
[64] T.A. Maia, J.M. Assaf, E.M. Assaf, Mater. Chem. Phys. 132 (2012) 1029.
[65] X.-S. Huang, H. Sun, L.-C. Wang, Y.-M. Liu, K.-N. Fan, Y. Cao, Appl. Catal. B: Environ. 90 (2009) 224–232.
[66] G. Xin, W. Guo, T. Ma, Appl. Surf. Sci. 256 (2009) 165–169.
[67] V.M. Shinde, G. Madras, Catal. Today 198 (2012) 270–279.
[68] P.A. Deshpande, S. Polisetti, G. Madras, AIChE J. 58 (2012) 932–945.
[69] K. Azzam, I. Babich, K. Seshan, L. Lefferts, Appl. Catal. B: Environ. 80 (2008) 129–140.
[70] K.I. Hadjiivanov, Catal. Rev.–Sci. Eng. 42 (2000) 71–144.
[71] H.-J. Freund, M.W. Roberts, Surf. Sci. Rep. 25 (1996) 225–273.
[72] E.-M. Köck, M. Kogler, T. Bielz, B. Klötzer, S. Penner, J. Phys. Chem. C 117 (2013) 17666–17673.
[73] M.S. Islam, G. Balducci, Catalysis by Ceria and Related Materials, in: A. Trovarelli (Ed.), Catalytic Science Series, vol. 2, Imperial College Press, 2013, pp. 281–309, Ch. 8.
[74] R. Burch, M.D. Coleman, Appl. Catal. B: Environ. 23 (1999) 115–121.
[75] M. Machida, D. Kurogi, T. Kijima, J. Phys. Chem. B 107 (2003) 196–202.
[76] I. Atribak, A. Bueno-Lopez, A. García-García, B. Azambre, Phys. Chem. Chem. Phys. 12 (2010) 13770–13779.
[77] I. Atribak, B. Azambre, A. Bueno López, A. García-García, Appl. Catal. B: Environ. 92 (2009) 126–137.
[78] W.F. Schneider, K.C. Hass, M. Miletic, J.L. Gland, J. Phys. Chem. B 106 (30) (2002) 7405–7413.
[79] M. Saito, M. Itoh, J. Iwamoto, K.-I. Machida, Chem. Lett. 37 (2008) 1210–1211.
[80] H. Xu, Q. Zhang, C. Qiu, T. Lin, M. Gong, Y. Chen, Chem. Eng. Sci. 76 (2012) 120–128.
[81] F.J.P. Schott, P. Balle, J. Adler, S. Kureti, Appl. Catal. B: Environ. 87 (2009) 18–29.